Copper and Nickel Complexes of Oxamate-Phenol Containing Ligands: A Structural Dichotomy in Oxidized Species

Guanqi Wang, Yohann Moreau, Florian Berthiol, Christian Philouze, Olivier Jarjayes, Fabrice Thomas

EurJIC
European Journal of Inorganic Chemistry

Research Article
doi.org/10.1002/ejic.202200781

Chemistry Europe
European Chemical Societies Publishing

www.eurjic.org

Copper and Nickel Complexes of Oxamate–Phenol Containing Ligands: A Structural Dichotomy in Oxidized Species

Guanqi Wang,[a] Yohann Moreau,[b] Florian Berthiol,[a] Christian Philouze,[a] Olivier Jarjayes,*[a] and Fabrice Thomas*[a]

The copper and nickel complexes of two tetradentate ligands derived from bis(aminophenol) and bis(phenol) architectures connected by an oxamate linker were isolated. Depending on the metal and ligand, the complex is isolated with either an intact (deprotonated) ligand ($\mathbf{1}^{2-}$), one-electron oxidized ligand ($\mathbf{2}^{-}$) or quinone form (**3**). Surprisingly, the Mannich base is easier to oxidize than the amidophenol derivatives. The complexes were characterized by X-ray diffraction, cyclic voltammetry, UV-Vis-NIR and EPR spectroscopies. Complex **1** shows two reversible oxidation waves assigned to the successive iminosemiquinone/aminophenolate redox systems. Complex $\mathbf{2}^{-}$ shows an intense NIR feature, as well as an EPR signal at $g_{iso} = 2.043$, consistent with a metallic contribution to the main ligand radical SOMO. Complex **3** shows the typical feature of an isolated Cu(II) complex. Spectro-electrochemistry coupled to DFT calculations demonstrate a ligand-centered oxidative redox chemistry for all the complexes.

Introduction

Sterically hindered phenolates and amidophenolates are prototypical examples of redox-active ligands.[1] Single electron oxidation affords phenoxyl or iminosemiquinonate radicals that can be persistent enough for structural characterization by X-ray diffraction, depending on the substitution pattern.[2] Amidophenolates are more electron-rich than phenolates, and hence usually require much lower potentials to be oxidized.[1] All these moieties have been intensively investigated in the early 2000's in the context of the modeling of galactose oxidase.[1–3] The active site of this enzyme indeed features a Cu(II)–tyrosyl site,[3a–g,4] despite it was initially believed to contain a Cu(III)–phenolate entity.[5] The factors that govern the oxidation site in complexes based on redox-active metals and ligands are numerous. It can obviously be the metal itself, but also the electronics of the redox-active group, the coordination sphere, and the nature of the donors in polydentate ligands.[1] These effects have been documented in copper complexes, which can afford either Cu(III) or Cu(II)–phenoxyl species upon oxidation. The first effect has been detailed in Cu(II)–salen complexes and it is now well established that the most electron-donating substituents favour ligand-centered oxidations, and hence phenoxyl species.[6] The second effect is comparatively less easy to anticipate, but it has been observed that the size of the chelation rings and the geometry of the metal ion can both influence the oxidation site.[7] Regarding the nature of the donors, a prototypical function dedicated to the stabilization of Cu(III) is the amidate.[8] It has been further used to get access to other high-valent metal ions of the first row such as Cr(V),[9] Mn(V)[10] Fe(IV),[11] Fe(V),[12] Co(IV),[13] and Ni(III).[14]

Surprisingly, only few complexes combine both the amidate function and electron-enriched phenol (or aminophenol) moieties (Figure 1,2). This association would afford easy-to-oxidize complexes, while inducing a duality in oxidation site. Representative examples of phenol–amidate conjugates are salen derivatives wherein the imine linker was substituted by an

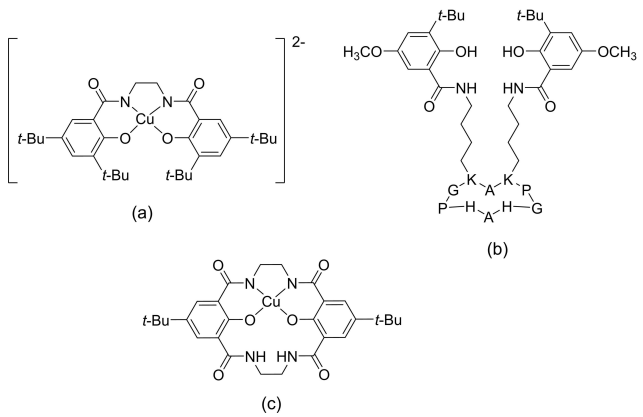

Figure 1. Structures of copper complexes combining both amidate functions and electron-rich phenols: (a) from [15]; (b) from [16]; (c) from [17].

[a] G. Wang, Dr. F. Berthiol, Dr. C. Philouze, Dr. O. Jarjayes, Prof. F. Thomas
Univ. Grenoble Alpes, CNRS
DCM, 38000 Grenoble (France)
E-mail: Olivier.jarjayes@univ-grenoble-alpes.fr
fabrice.thomas@univ-grenoble-alpes.fr
[b] Dr. Y. Moreau
Univ. Grenoble Alpes, CEA
CNRS, IRIG-LCBM, 38000 Grenoble (France)

Supporting information for this article is available on the WWW under https://doi.org/10.1002/ejic.202200781

Research Article
doi.org/10.1002/ejic.202200781

amide (Figure 1a),[13a,15,18] cyclic peptides appended by di-*tert*-butyl–amidophenol moieties (Figure 1b)[16] or the bis-(2-hydroxyisophtalamide) macrocyclic ligand developed by Benisvy et al. that was chelated to zinc and copper (Figure 1c).[17] Some aminophenol–amide conjugates were built through the connection of two aminophenols moieties by a bis(oxamate) linker (tetradentate H_4L_1, Figure 2). The coordination chemistry and redox properties of the gallium and iron complexes of H_4L_1 was investigated by Wieghardt et al..[19] In both complexes the bis(oxamate) unit adopts a *trans* configuration, leading to compounds with a (2:1) rather than (1:1) (M:L) stoichiometry (Figure 2). The donor set provided by the ligand is $N_{(amidate)}$-$O_{(phenolate)}O_{(amidate)}$ for each metal ion. Both complexes can undergo two successive single-electron oxidations assigned to ligand-centered redox events in the range 0.08 to 0.45 V vs. Fc^+/Fc. The same stoichiometry and donor set was later demonstrated for the tin and germanium complexes, but no electrochemical data was reported.[20] Dimerization into (4:2) structures was proposed for group 4 transition metal ions, but unfortunately no crystal structure was reported.[21] Finally, complexes with higher stoichiometries (6:2 and 8:2 M:L) were reported for the zinc complexes.[22]

In this article we reinvestigate the coordination chemistry of H_4L_1 with two divalent metals of the first row, copper and nickel. We establish that complexes of low stoichiometry, for example (1:1) (M:L), are accessible with this ligand framework: the oxalate adopts a *cis* conformation in this case, leading to monomeric structures wherein the ligand provides a N_2O_2 donor set. We also prepared the ligand H_4L_2 whose structure differs from H_4L_1 by the nature of the redox-active group, phenol instead of aminophenol. A mononuclear copper complex of similar stoichiometry and donor set was isolated. Against all expectations, the amidophenolate groups are more robust towards oxidation than the Mannich base.

Results and Discussion

Synthesis and structures

Ligand H_4L_1 was synthesized according to a published procedure.[19] Ligand H_4L_2 was prepared by mixing 1 equivalent of diethyl oxalate and 2 equivalents of 2-aminomethyl-4,6-di-*tert*-butylphenol. The ligand H_4L_1 was chelated to $Cu(OAc)_2$ and $Ni(OAc)_2$ in MeOH in the presence of 4 molar equivalents of base $(N(n\text{-}Bu)_4)(OH)$. Slow evaporation of a concentrated solution of each complex affords single crystals of $[Cu(L_1)](N(n\text{-}Bu)_4)_2$ (**1**$(N(n\text{-}Bu)_4)_2$) and $[Ni(L_1)](N(n\text{-}Bu)_4)$ (**2**$(N(n\text{-}Bu)_4)$), respectively. When H_4L_2 is chelated to copper under similar conditions the neutral complex $[Cu(L_2)]$ (**3**) was isolated and crystallized. We additionally conducted the synthesis of the nickel complex of H_4L^1 in the glovebox: The complex (**2**$(N(n\text{-}Bu)_4)_2$) could be isolated as an air sensitive powder. Despite our efforts it was not possible to isolate this compound as single crystals suitable for X-ray diffraction.

The crystal structures of **1**$(N(n\text{-}Bu)_4)_2$, **2**$(N(n\text{-}Bu)_4)$ and **3** are depicted in Figure 3, while selected bond distances are summarized in Table 1. In all the complexes the metal ion lies in a N_2O_2 coordination environment. It is mostly square planar, as demonstrated by N1CuO2 and N2CuO1 angles (or N1CuO1′ and N1′CuO1) within the range 168–176°.

The crystal cell of $\mathbf{1}^{2-}$ contains three distinct molecules, with very similar structures, as well as six molecules of counter-ion (tetra-*n*-butylammonium) for the electroneutrality. The Cu–N bond distances range between 1.900 and 1.911 Å, as expected for amidate ligation, while the Cu–O ones are within the range 1.930–1.953 Å. The absence of quinoidal alternance of bond lengths within the peripheral rings, as well as the long C–O bond (1.334–1.357 Å) strongly support an amidophenolate

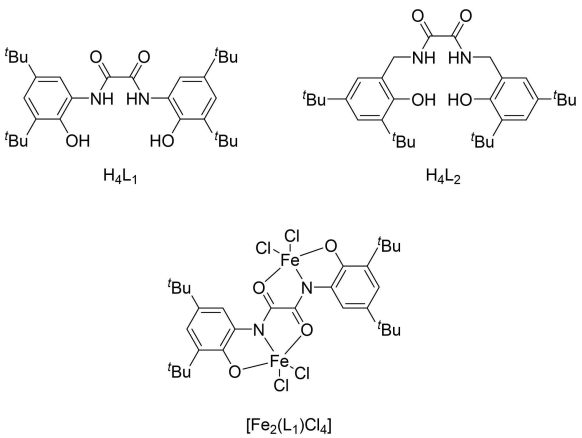

Figure 2. Structures of the ligands and the iron complex reported by Wieghardt et al. for deprotonated $(L_1)^{4-}$.[19]

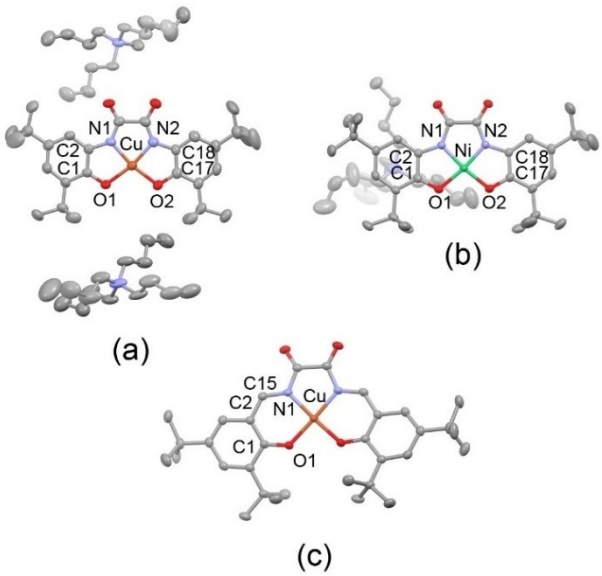

Figure 3. ORTEP views of (a) **1**$(N(n\text{-}Bu)_4)_2$, (b) **2**$(N(n\text{-}Bu)_4)$ and (c) **3**. The hydrogens and counter ions are omitted for clarity. Depicted with 50% thermal ellipsoids.

Research Article
doi.org/10.1002/ejic.202200781

Table 1. Selected bond lengths (Å) in the complexes.[a]

	Complex **1**[a]	Complex **2**	Complex **3**
M–O1	1.930(3)	1.846(2)	1.900(2)
	1.953(4)	1.836(2)	
	1.943(4)		
M–O2	1.942(3)	1.851(2)	
	1.942(4)	1.840(2)	
	1.935(3)		
M–N1	1.904(4)	1.808(2)	1.923(2)
	1.900(5)	1.806(2)	
	1.910(5)		
M–N2	1.903(4)	1.806(2)	
	1.910(5)	1.805(2)	
	1.911(4)		
O1–C1	1.334(6)	1.337(1)	1.290(2)
	1.357(7)	1.329(3)	
	1.350(6)		
O2–C17	1.348(6)	1.330(3)	
	1.339(6)	1.333(3)	
	1.343(6)		
N1–C2	1.400(6)	1.390(3)	n/a
	1.393(7)	1.393(3)	
	1.399(7)		
N2–C18	1.413(6)	1.394(3)	
	1.401(6)	1.385(3)	
	1.405(7)		

[a] From X-ray diffraction analysis. [b] Three molecules of complex are present in the crystal cell. [c] two molecules of complex are present in the crystal cell.

formulation of the redox-active rings. Hence, complexation was not accompanied by oxidation of the ligand, as usual for amidophenolate derivatives chelated to divalent metals ions.[23] The oxamate linker likely contributes to an increase in the iminosemiquinonate/amidophenolate redox potential, explaining this peculiar behaviour of H_4L_1.

The crystal cell of the nickel complex $\mathbf{2}^-$ contains two distinct molecules, which once again exhibit very similar structures. It must be stressed that a single molecule of tetra-*n*-butylammonium is present per molecule of complex, demonstrating a formal charge distinct from that of the copper derivative. The C1–O1 and C17–O2 bonds are usually the hallmarks of the ligand oxidation state in amidophenolate derivatives. These bonds are within the range or slightly smaller than the corresponding ones in $\mathbf{1}^{2-}$. On the other hand the quinoidal distribution of bond distances expected for iminosemiquinonate radicals or iminoquinones is hardly observed in $\mathbf{2}^-$. We take this as strong support for ligand radical formation, wherein the SOMO is delocalized over both peripheral rings. This behavior indeed contributes to the dilution of the bonding rearrangements with the whole organic framework. It is worth noting that the coordination sphere in $\mathbf{2}^-$ is contracted with respect to $\mathbf{1}^{2-}$, mostly due to the different ionic radius of the nickel ion.

Complex **3** shows a symmetrical coordination sphere, with the bond distances Cu–O1 and Cu–N1 at 1.900 and 1.923 Å, respectively. The shortening of the Cu–O1 bond, when compared to $\mathbf{1}^{2-}$, likely arises from the formation of 5:6:5 chelate rings instead of a 5:5:5 one, which favours the positioning of the O donors closer one with each other, and closer to the metal center. The crystal cell is exempt from any counter-ion, demonstrating that the complex is neutral. This important observation shows that both peripheral rings of H_4L_2 underwent two-electron oxidation during the synthesis, in contrast to H_4L_1. Note that the yield in isolated product is 27% and the reaction is reproducible. Hence **3** is not a minor degradation product whose crystallization was fortuitous. Two plausible limit structures can account for the neutral character of **3**: Cu(III) coordinated to a monooxidized ligand radical (Figure 4a) or Cu(II) coordinated to a dioxidized ligand or ligand half (Figure 4b,c).[24] In this latter case the ligand is either radical (bis(phenoxyl) species, Figure 4b) or closed-shell (Figure 4c). The C1–O1 bond distance is 1.290 Å, which is below the values typically reported for coordinated phenolates (see $\mathbf{1}^{2-}$), while a quinoidal alternance of bond distances is observed in both peripheral rings, both confirming that the ligand is oxidized. Most importantly, the C2–C15 bond is 1.404 Å, which is too short for a genuine single bond (ca. 1.50 Å in Mannich bases).[25] In addition, a single hydrogen atom bonded to C15 was clearly seen on the difference Fourier map. These structural features compare fairly well with those reported for quinone methides or keto-enamine units:[,26b,27] In the keto-enamine form of the 2,3-bis(salicylideneamino)-1,4-butanediol the C=O bond distances is indeed 1.293(3) Å, while the C–C bond distance analog to C2–C15 is 1.429(3) Å.[26] In the keto-enamine form of 2-[(2-hydroxybenzylidene)amino]pyridin-3-ol the corresponding C=O and C–C bond lengths are 1.298(2) and 1.412(2) Å, respectively.[27] Finally, the O1, C1, C2, C15, N1 atoms are almost coplanar, with a deviation of the C15 atom from the mean plane of only 0.026 Å. All these data point towards a bis-oxidation of each ligand half into the structure depicted in Figure 2c. Note that the oxidation is accompanied by proton transfers (PCET).

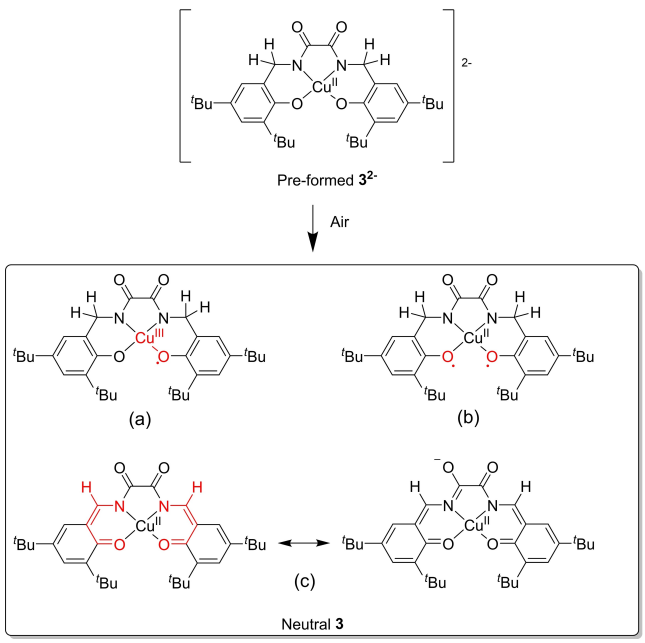

Figure 4. Plausible structures for **3**. Structure c is that identified at the solid state.

Research Article
doi.org/10.1002/ejic.202200781

Electrochemistry

The electrochemical behavior of **1**(N(*n*-Bu)$_4$)$_2$, **2**(N(*n*-Bu)$_4$) and **3** has been investigated by cyclic voltammetry (CV), differential pulse voltammetry (DPV) and rotating disc electrode (RDE) voltammetry in CH_3CN (Figure 5, Table 2) and methanolic solutions (Supporting Information, Table 2) containing TBAP as supporting electrolyte. The CV of $\mathbf{1}^{2-}$ in CH_3CN (Figure 5a) shows two oxidation waves. The first is reversible and observed at $E_{1/2}{}^1 = -0.45$ V vs. Fc^+/Fc in CH_3CN. The second one is irreversible and detected at $E_p{}^2 = -0.08$ V. Based on RDE voltammetry they are assigned to one-electron process each. The two redox waves are thus assigned to successive oxidations of the amidophenolate rings into iminosemiquinonate moieties (Scheme 1). It is significant that the resting potential is close to −0.4 V for $\mathbf{1}^{2-}$ after 30 min in air, with an intensity of the first oxidation wave that is inferior to the second one. Furthermore, the open circuit potential is not observed at a plateau in the RDE curve but at potential jump, at a value close to $E_{1/2}{}^1$. This demonstrates a slow oxidation of $\mathbf{1}^{2-}$ into $\mathbf{1}^-$ in the electrolytic medium. From the ratio of intensities, it is calculated that after 30 min about one half of the complex is under its one-electron oxidized form $\mathbf{1}^-$ (likely oxidized by air), the remaining part being under its initial oxidation state $\mathbf{1}^{2-}$ (see Supporting Information). This slow oxidation is in line with the low $E_{1/2}{}^1$ value. It is worth noting that these potentials are significantly more negative than in the reported Fe^{III} and Ga^{III} complexes, which did not show such behaviour. Both the smaller metal formal charge and differences in the coordination spheres (dimer vs. monomer) could explain this difference.

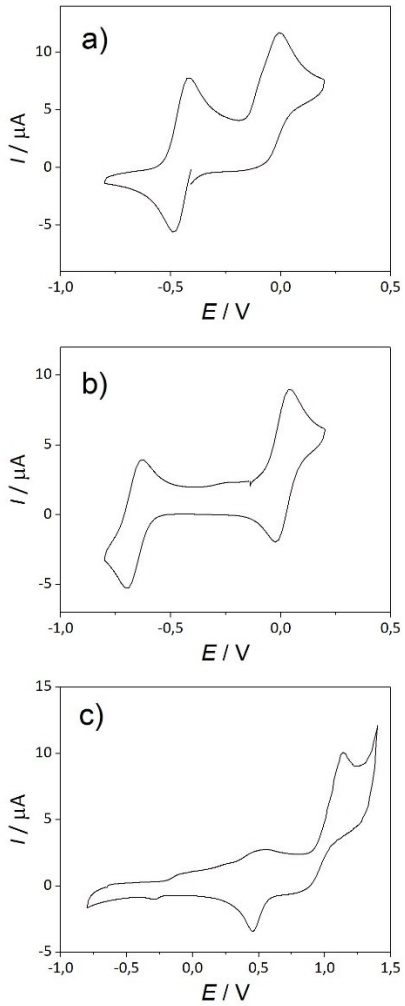

Figure 5. Cyclic voltammetry curves of 0.5 mM CH_3CN solutions (+0.1 M TBAP) of: a) **1**(N(*n*-Bu)$_4$)$_2$; b) **2**(N(*n*-Bu)$_4$) and c) **3** at a carbon electrode. Scan rate = 0.1 V/s, T = 298 K. The potentials are given relative to the Fc^+/Fc redox couple that was used as external reference.

Table 2. Electrochemical data of the complexes.

Complex[a]	$E_{1/2}{}^1$ [V]	ΔE_p [V]	$E_{1/2}{}^2$ [V]	ΔE_p [V]
1(N(*n*-Bu)$_4$)$_2$[a]	−0.45	0.07	−0.08[b]	–[b]
2(N(*n*-Bu)$_4$)$_2$[a]	−0.66	0.07	0.01	0.08
1(N(*n*-Bu)$_4$)$_2$[c]	−0.25	0.07	−0.01	0.07
2(N(*n*-Bu)$_4$)$_2$[c]	−0.46	0.08	0.06	0.08
$[Ga_2(L_1)(Cl)_4]^{2-}$	0.08[d]		0.35[d]	
$[Fe_2(L_1)(Cl)_4]^{2-}$	0.16[d]		0.45[d]	
3[a]	1.14, 0.42[e]	–[e]		–

[a] in CH_3CN + 0.1 M TBAP. T = 298 K, potentials given vs. Fc^+/Fc. [b] Irreversible process, only the $E_p{}^a$ value is given and no ΔE_p is provided. [c] in CH_3OH + 0.1 M TBAP. [d] In CH_2Cl_2 containing TBAP at 243 K. From Ref. [28]. [e] Main oxidation and reduction peaks ($E_p{}^a$ and $E_p{}^c$).

The CV curve of complex $\mathbf{2}^-$ also exhibits two reversible waves, with somewhat distinct potentials ($E_{1/2}{}^1 = -0.66$ and $E_{1/2}{}^2 = 0.01$ V). As for $\mathbf{1}^{2-}$ they are assigned to redox processes mostly centered on the amidophenolate rings. The significantly lower $E_{1/2}{}^1$ value in this case points to distinct spin distribution in $\mathbf{1}^-$ that we assign to a non-negligible metal contribution to the main radical SOMO (see below). The resting potential of $\mathbf{2}^-$ is measured between $E_{1/2}{}^1$ and $E_{1/2}{}^2$, with a zero current at the plateau between the two redox waves. Clearly, one redox wave is an oxidation one, the other a reduction one and the solution is not composed of a mixture of two oxidation states even after hours, in contrast with $\mathbf{1}^{2-}$. This different behavior is explained by the lower $E_{1/2}{}^1$ value of $\mathbf{2}^-$ in comparison to $\mathbf{1}^{2-}$, and the subsequent isolation of the first complex already under its monoanionic form.

We additionally performed electrochemical measurements in methanol, which is the solvent used for the crystallization of the complexes (Supporting Information). The same trend in potentials was observed between the complexes, whereby the nickel complex is 0.2 V easier to oxidize than the copper one. Interestingly, the potentials are anodically shifted by about 0.2 V when compared to acetonitrile (Table 2), which also explains why the copper complex did not undergo significant oxidation during the crystallization process. Altogether, these data confirm that $\mathbf{2}^-$ could be isolated as an anion at the solid state (in air), whereas the copper complex crystallized under the form of a dianion under similar conditions.

$$[Cu^{II}(L^1)]^{2-} \overset{E_{1/2}{}^1}{\rightleftharpoons} [Cu^{II}(L^1)]^{\bullet-} \overset{E_{1/2}{}^2}{\rightleftharpoons} [Cu^{II}(L^1)]^{2\bullet}$$

Scheme 1. Redox processes for $\mathbf{1}^{2-}$.

Research Article
doi.org/10.1002/ejic.202200781

The CV curve of **3** contrasts sharply with the two other ones. It shows oxidation waves at $E_p^a = 0.49$ V and 1.14 V. A cathodic peak was observed at $E_p^c = 0.42$ V in the reverse scan. This suggests that a chemical reaction is coupled to oxidation and that the oxidation product is unstable. Controlled potential electrolysis at 233 K confirmed the low stability of the oxidized species, as demonstrated by a dramatic decrease in intensity of both redox waves, together with the appearance of a new cathodic peak at −0.79 V (see Supporting Information).

EPR spectroscopy

The EPR spectra of the copper complexes in CH_3CN solution containing TBAP are depicted in Figure 6, while data are summarized in Table 3. The spectrum of a solution of the crystals of **1**(N(*n*-Bu)$_4$)$_2$ freshly dissolved in the electrolytic acetonitrile medium exhibits the expected features of a magnetically isolated mononuclear copper complex (Figure 6a). The spectrum is remarkably unchanged upon substituting acetonitrile by methanol, which excludes axial ligation by the solvent. The spin Hamiltonian parameters determined by simulation are $g_{//} = 2.177$, $g_{\_|\_} = 2.042$, $A(Cu)_{//} = 640$, $A(Cu)_{\_|\_} =$ 110 MHz. Bulk electrolysis at an applied potential slightly above $E_{1/2}$[1] results in a quenching of the copper resonances, indicative of magnetic interactions between the copper spin and the ligand radical. No resonance could be detected, indicative of either a triplet ground spin state with large zero field splitting parameters,[6c] or a diamagnetic ground state. Further oxidation at 0.2 V results in the appearance of isolated copper resonances. The intensity is however weaker than expected for the full conversion of **1**$^-$ into an isolated ($S = 1/2$) system. This behavior is consistent with the poor reversibility of the second oxidation wave of **1**$^{2-}$, and hence the observation of decomposed species.

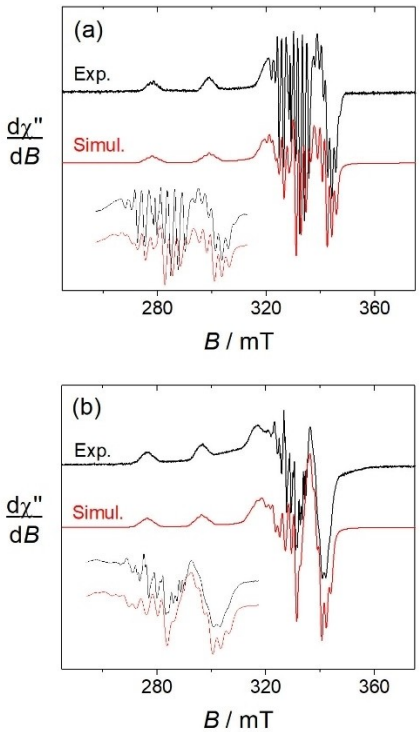

Figure 6. X-Band EPR spectra of 0.5 mM CH_3CN solutions (+0.1 M TBAP) of: a) **1**(N(*n*-Bu)$_4$)$_2$ (black) and b) complex **3**. Black lines are experimental spectra, red lines represent simulations using the parameters given in Table 3. The inset represents a magnified view of the perpendicular region. Microwave Freq. 9.43 GHz, power 5 mW; Mod. Amp. 0.3 mT, Freq. 100 KHz. $T = 100$ K.

Table 3. EPR data of the complexes.

Complex[a]	g values	A values (MHz, Cu nucleus)
1^{2-}	2.177, 2.045, 2.045	640, 100, 100
1$^-$	silent	n/a
2^{2-}	silent	n/a
2$^-$	2.117, 2.007, 2.007	n/a
2	silent	n/a
3	2.197, 2.042, 2.042	620, 110, 110

[a] in CH_3CN + 0.1 M TBAP. $T = 100$ K.

The spectrum of **2**(N(*n*-Bu)$_4$) in CH_3CN (+TBAP) is shown in Figure 7. It is characterized by an axial ($S = {}^1/_2$) system with $g_{//} =$ 2.117 and $g_{\_|\_} = 2.007$. The g_{iso} value is 2.043, which is slightly higher than that of free phenoxyl radicals ($g_{iso} = 2.004$),[29] but far below that expected for Ni(III) complexes ($g_{iso} = 2.10$–2.15)[6a,18a,30] This demonstrates a main radical character of **2**$^-$, with a somewhat non-negligible contribution of an out-of-plane metal d orbital to the SOMO.[2c,d] There is no significant spectral change whether **2**$^-$ is dissolved in acetonitrile or methanol, ruling out any valence tautomerism induced the alcohol coordination. Both **2**$^{2-}$ (prepared in the glove box) and **2** proved to be X-band EPR silent.

Complex **3** shows a typical copper spectrum (Figure 6b). It could be simulated by considering an axial signal with $g_{//} =$ 2.197, $g_{\_|\_} = 2.042$, $A(Cu)_{//} = 620$, $A(Cu)_{\_|\_} = 110$ MHz (and including hyperfine interaction with two ^{14}N atoms $A(2\,N)_{iso} =$ 50 MHz), consistent with the limit structure c depicted in Figure 2. The $g_{//}/A_{//}$ratio is 106 cm, for example close to **1**$^{2-}$ (102 cm), consistent with a similar square planar geometry of the metal center.

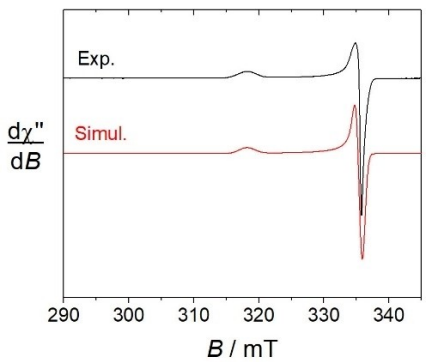

Figure 7. X-Band EPR spectrum of a 0.5 mM CH_3CN solution (+0.1 M TBAP) of **2**$^-$. The black line represents the experimental spectrum, the red line represents a simulation using the parameters given in the text. Microwave Freq. 9.43 GHz, power 5 mW; Mod. Amp. 0.3 mT, Freq. 100 KHz. $T = 100$ K.

Research Article
doi.org/10.1002/ejic.202200781

Electronic structures by DFT calculations

The electronic structure of the complexes under various oxidation states has been investigated by DFT calculations. The experimental coordination sphere (from crystal structure determination) proved to be adequately reproduced by using the TPSSh functional, with variations that do not exceed 0.024 Å.

The SOMO of the copper complex $\mathbf{1}^{2-}$ is mainly developed on the metal center, consistent with its formulation as a Cu(II) ion coordinated to a diamagnetic ligand. For the corresponding anion $\mathbf{1}^{-}$ we considered three configurations: a genuine closed-shell singlet (Cu(III)), a triplet and a broken-symmetry singlet (both are Cu(II)-radical). The energetic analysis disclosed that the triplet is the most stable state with an energy gap between the triplet and the Cu(III) state of 6.3 kcal/mol. This confirms that complex $\mathbf{1}^{-}$ is best described as a Cu(II)-radical system (Figure 8a).

The nickel complex $\mathbf{2}^{2-}$ was confirmed to be a low spin Ni(II) bound to a diamagnetic ligand. The anion $\mathbf{2}^{-}$ is a doublet system, whose SOMO is mainly developed on the ligand framework (90%, Figure 8b), with a contribution of the metal center calculated at 10%. The metal contribution to the SOMO arises from a mixing between the ligand radical π orbital and a d orbital with appropriate symmetry, for example d_{xz} or d_{yz}. The SOMO is equally shared between the two peripheral rings (mixed-valent radical character). The EPR parameters were also computed, leading to $g_x = 2.002$, $g_z = 2.016$ and $g_y = 2.111$, in good agreement with experimental data. Regarding neutral **2** the calculations point to a singlet spin state, the triplet being located 6.5 kcal/mol above. The electronic structure is however not straightforward, as DFT predicts both the closed-shell and open-shell singlets to be essentially isoenergetic.

The last complex, **3**, was investigated under a doublet spin state and not surprisingly DFT calculations support a main metal-centered SOMO. We further investigated the oxidation site of **3** by calculating the electronic structure of $\mathbf{3}^{+}$ under both its singlet and triplet spin states. The latter proved to be 5.3 kcal/mol lower in energy than the first, demonstrating a ligand-centered redox process. The spin density in the triplet $\mathbf{3}^{+}$ is delocalized over the ligand (43%) and copper (57%) atom, providing to the complex a main Cu(II)-radical character. Note that this calculation refers to an intermediate that rapidly evolves and could not be characterized by spectro-electrochemistry.

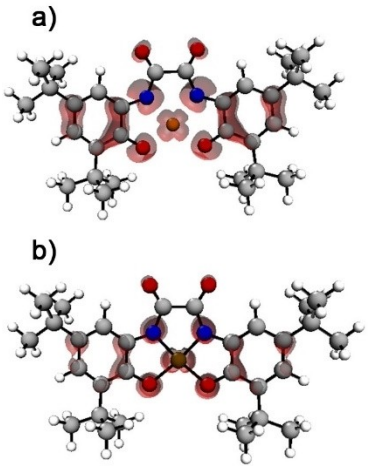

Figure 8. Spin density plots for: a) $\mathbf{1}^{-}$ and b) $\mathbf{2}^{-}$ (from a TPSSh/Def2SVP calculation).

UV-Vis-NIR spectroscopy and TD-DFT calculations

All the complexes are colored and their electronic spectra are depicted in Figure 9 and Figure S15. The spectral data are summarized in Table 4, while the electronic excitations predicted by DFT calculations are listed in Table 5.

The electrolytic solution of $\mathbf{1}(N(n\text{-}Bu)_4)_2$ is characterized by an intense band at 402 nm together with a less intense one at 559 nm (Figure 9a). They are assigned to βHOMO-4→βLUMO and βHOMO→βLUMO+1 by TD-DFT calculations (Figure 10a). Electrochemical oxidation of $\mathbf{1}^{2-}$ into $\mathbf{1}^{-}$ produces a chromophore with two main bands at 386 and 477 nm (5167 $M^{-1}\,cm^{-1}$ and 2918 $M^{-1}\,cm^{-1}$ respectively). Based on calculations they correspond to α HOMO-1→α LUMO and α HOMO→α LUMO, respectively ($\lambda_{clcd} = 379$ and 462 nm, Figure 10b). Further oxidation of $\mathbf{1}^{-}$ results in a simplification of the spectrum, with a weak band at 416 nm (734 $M^{-1}\,cm^{-1}$, Figure 9a). The TD-DFT spectrum computed for complex **1** by assuming a geometry

Table 4. Vis-NIR data of the complexes.

Complex[a]	λ_{max} [nm] (ε [$M^{-1}\,cm^{-1}$])
$\mathbf{1}^{2-}$	265 (24193), 338 (6737), 402 (5370), 559 (289)
$\mathbf{1}^{-}$	251 (17990), 275 (17506), 386 (5167), 477sh (2918)
1 [b]	277 (10160), 416 (734)
$\mathbf{2}^{2-}$ [c]	277 (23914), 331 (12270), 451 (2490), 484 (2206), 554sh (1030)
$\mathbf{2}^{-}$	274 (16970), 328 (8000), 355sh (5283), 418 (1763), 494 (973), 535 (996), 592 (638), 729 (288), 1090sh (6201), 1200 (8919), 1295sh (7507)
2	270 (14320), 337 (4840), 406 (2720), 445sh (1230), 595 (611), 957 (14060), 1065sh (6083)
3	263 (8907), 339 (3824), 470 (1150)

[a] in CH_3CN + 0.1 M TBAP. $T = 298$ K. [b] Corresponds to a decomposition product (see the text). [c] Generated in the glovebox.

Table 5. Electronic excitations predicted by DFT calculations.[a]

Complex	λ_{clcd} [nm] (f_{osc})	Assignment [C in %][b]
$\mathbf{1}^{2-}$	388 (0.039),	β-HOMO-4→β-LUMO (68%)
	532 (0.0008)	β-HOMO→β-LUMO+1 (52%)
$\mathbf{1}^{-}$	379 (0.031)	α-HOMO-1→α-LUMO (36%)
	462 (0.095)	α-HOMO→α-LUMO (71%)
$\mathbf{2}^{2-}$	404 (0.0251)	HOMO-5→LUMO+1 (71%)
	544 (0.0626)	HOMO→LUMO (98%)
$\mathbf{2}^{-}$	1008 (0.246)	β-HOMO→β-LUMO (80%)
2	837 (0.518)	HOMO→LUMO (95%)
3	508 (0.0826)	β-HOMO-2→β-LUMO+1 (60%)

[a] From a TD-DFT calculation (TPSSh/Def2svp/PCM). [b] The percentage contribution C is expressed as the ratio between the square of the coefficient for a given excitation divided by the sum of the square of the coefficients for all the excitations.

Research Article
doi.org/10.1002/ejic.202200781

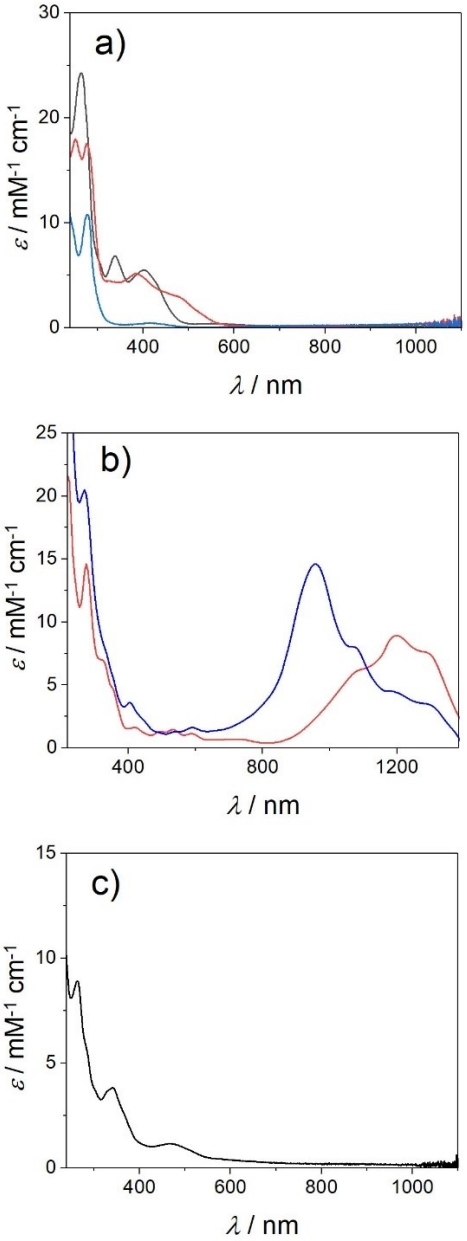

Figure 9. UV-Vis-NIR spectra of 0.5 mM CH_3CN solutions (+0.1 M TBAP) of the complexes: a) $\mathbf{1}^{2-}$ (black), $\mathbf{1}^{-}$ (red) and **1** (blue); b) $\mathbf{2}^{-}$ (red) and **2** (blue); c) **3** (black). $T = 298$ K, $l = 1.000$ cm.

identical to $\mathbf{1}^{-}$ was also generated but no correspondence with the experimental absorption spectrum could be found. A possible reason is that the experimental spectrum is that of an unidentified product originating from the fast evolution of **1** (see above).

The nickel complex **2**(N(*n*-Bu)$_4$) dissolved in CH_3CN demonstrates a rich visible spectrum, with at least five distinct transitions between 400 and 800 nm, as well as an intense NIR feature centered around 1200 nm (Figure 9b). This latter is assigned to β-HOMO→β-LUMO by calculations (λ_{clcd} = 1008 nm), which is a ligand-to-ligand charge transfer involving the peripheral rings (the transitions are summarized in Figure S17). The spectrum after one-electron oxidation (formation of **2**) is dominated by a band at 957 nm (14 060 $M^{-1}\,cm^{-1}$), which is attributed to HOMO→LUMO (λ_{clcd} = 837 nm). The dianionic precursor $\mathbf{2}^{2-}$ does not show any intense NIR band, but a shoulder at ca. 550 nm, as well as two bands at 451 and 484 nm (Figure S18). Accordingly, TD-DFT calculations do not predict any electronic excitation in the NIR region for this species. Conversely, transitions are computed at 544 nm (HOMO→LUMO) and 404 nm (mostly HOMO-5→LUMO + 1), which are attributed to the experimental bands at 484 nm and 451 nm, respectively (Figure S19).

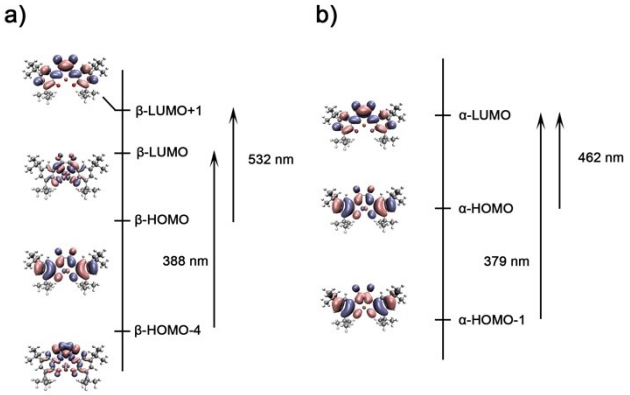

Figure 10. Predicted electronic excitations for (a) $\mathbf{1}^{2-}$ and (b) $\mathbf{1}^{-}$ from a TD-DFT calculation (TPSSh/Def2svp/PCM).

Finally, the experimental visible spectrum of **3** consists of a main absorption located at 470 nm, which is assigned to β-HOMO-2→β-LUMO + 1 (λ_{clcd} = 508 nm) by TD-DFT.

Alcohol oxidation

The galactose oxidase-like reactivity of the copper complexes has been investigated towards aerobic alcohol oxidation. The complexes were dissolved in CH_2Cl_2 containing the alcohol, with or without exogenous base. The reaction mixture was stirred under dioxygen at 298 K and the products were analyzed. The results are summarized in Table 6.

The first substrate to be investigated was benzyl alcohol. For all the complexes a strong base (suspension of tBuOK) proved to be essential for catalysis, as no TONs is achieved even after 24 h reaction in its absence. This demonstrates the need for alcohol deprotonation for an efficient catalysis. The hydroxyl deprotonation indeed both favours its binding onto the metal and lowers the energy of the C–H bond in α position of the hydroxyl.[3c,d,31] The reaction in the presence of tBuOK proceeds rapidly to produce benzaldehyde with TONs of 108 and 87 ($\mathbf{1}^{2-}$ and **3**) at 1 h, which is significantly higher than copper acetate in solution (20). The TONs do not vary much during 6 h, with values of 90 and 104, respectively. When the copper(II) complex of H_4L_2 was pre-formed in the glovebox and used as catalyst instead of **3** the TON was slightly higher, with TONs of 162 and 131 after 1 and 6 h, respectively. The yield is almost constant or

Research Article
doi.org/10.1002/ejic.202200781

Table 6. Catalytic activity of the complexes.[a]

Complex	Substrate	TON[c] (benzaldehyde/benzoate) 1 h	3 h	6 h	24 h
$\mathbf{1}^{2-}$	Benzyl alcohol	108/18	95/34	90/48	103/78
3	Benzyl alcohol	87/6	108/28	104/73	138/115
3 [b]	Benzyl alcohol	162/29	139/52	131/105	188/170
$Cu(OAc)_2$	Benzyl alcohol	20/24	30/30	44/36	84/64
$\mathbf{1}^{2-}$	2-phenylethanol	0	0	0	0
3	2-phenylethanol	0	0	13	23
3 [b]	2-phenylethanol	18	21	60	33
$Cu(OAc)_2$	2-phenylethanol	0	0	0	0

[a] 0.08% in catalyst (0.5 mM), 0.6 M in alcohol, 1.2 equiv. of tBuOK in CH_2Cl_2 at 298 K under O_2. $T = 100$ K; [b] Copper(II) complex of H_4L_2 pre-formed in the glovebox; [c] The two TON values given for the oxidation of benzyl alcohol refer to benzaldehyde (first)/benzoate (second). The TON refers to 2-phenylacetaldehyde when 2-phenylethanol was used as substrate.

eventually decreases between 1 and 6 h, which prompted us to analyzed the suspension: An extraction of the reaction mixture with water allowed for the identification of potassium benzoate in large amount in the aqueous phase by ^{1}H NMR. No aldehyde peak could be detected, due to the low solubility of benzaldehyde in water. This demonstrates that the suspension is composed of both tBuOK and potassium benzoate, and the latter can be separated cleanly from benzaldehyde by a simple extraction. Hence the catalysts exhibit a glyoxal oxidase-like activity in addition to the targeted galactose oxidase one.[3f,32] It is worth noting that the TON for benzoate was largely inferior to benzaldehyde during the first hours of catalysis, but regularly increases with time. After 24 h the TONs approach that in benzaldehyde, with values of 78, 115 and 178 for $\mathbf{1}^{2-}$, **3** and the pre-formed copper complex of H_4L_2, respectively. Depending on the experimental protocol and reaction time it is thus possible to recover either benzaldehyde or benzoate. The reaction was monitored by UV-Vis spectroscopy for both $\mathbf{1}^{2-}$ and **3** (Figure S21). After 1, 3 and 6 h an aliquot was taken, filtered over celite and diluted into dichloromethane for UV-Vis analysis: After 1 h the features of $\mathbf{1}^{-}$ were detected, followed by a bleaching in the visible region. It was not possible to attest the formation of **1** due its low absorptivity above 300 nm and overlap with benzaldehyde absorption. Overall these data suggest that substrate oxidation generates a transient reduced complex that is rapidly reoxidized under dioxygen (at least into $\mathbf{1}^{-}$), which can be accumulated for detection. This implies that the rate limiting step during turnovers is the C–H bond activation of the substrate and not reoxidation of the catalyst, similarly to galactose oxidase.[3c] A transient species with an absorption band around 400 nm could be detected in the case of **3**, but it could not be attributed to any characterized chromophore.

We further screened the oxidation of the unactivated 2-phenylethanol. For **3** and the pre-formed copper complex of H_4L_2 the TONs are modest, 23 and 33, respectively (after 24 h), in line with the stronger C–H bond to be broken. No catalytic activity could be detected for $\mathbf{1}^{2-}$.

For both substrates the catalytic performance of the complexes follows the trend $\mathbf{1}^{2-} < \mathbf{3} <$ pre-formed copper complex of H_4L_2. The lower activity of $\mathbf{1}^{2-}$ appears surprising given the high catalytic activity reported for a derivative featuring a phenylene linker instead of the oxamate.[23f] It might be connected to the lack of redox participation of the bridge in the catalytic process, as well as a shift in redox potentials.

Conclusion

Three complexes were prepared from oxamate-based tetradentate N_2O_2 ligands featuring either amidophenols or phenol chelating groups. Unexpectedly, the latter moiety proved to be more sensitive to oxidation, resulting in the isolation in air of the copper complex under a highly stable Cu(II)–quinone form (Figure 11). We interpret this singularity by the fact that the amidate connectivity does not only lower the oxidation potential, but also provides a way for expending the conjugation in the oxidized ligand. In the other ligand family, the oxidation potentials are low and the metal affects them sufficiently for isolating complexes under distinct oxidation states: The copper complex was isolated with an intact ligand (two amidophenolate arms), whereas the nickel one was crystallized under its mixed amidophenolate/iminosemiquinone form, despite identical experimental conditions. In conclusion the amidate function, which is usually known for stabilizing trivalent copper, does not favours Cu(III) formation in the present series. A ligand-centered redox activity is observed with both phenol and aminophenol peripheral rings, demonstrating a dichotomy in the oxidation site when amidates are associated to redox-active ligands. Finally, complex **3** and its precursor demonstrate an interesting catalytic activity towards aerobic oxidation of benzyl alcohol: Benzaldehyde or benzoic acid could be recovered independently, the first being mainly formed at the early stage of the reaction and the other progressively along catalysis.

Experimental Section

Material and methods: All chemicals were of reagent grade and were used without purification. NMR spectra were recorded on a Bruker AM 400 (^{1}H at 400 MHz) spectrometer. Chemical shifts are quoted relative to tetramethylsilane (TMS). Mass spectra were recorded on an ESI/QTOF Waters Xevo G2-S apparatus. The FTIR spectra were recorded using a Nicolet iS10 spectrometer on

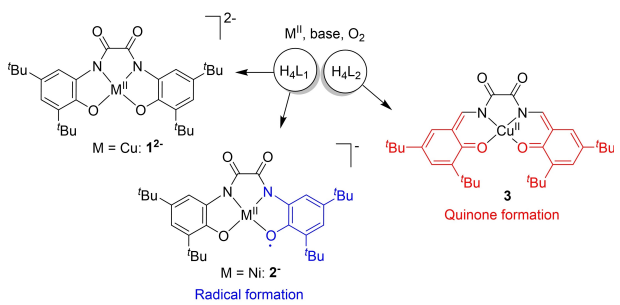

Figure 11. Complexes isolated from H_4L_1 and H_4L_2.

Research Article
doi.org/10.1002/ejic.202200781

crystalline material (ATR mode). UV/Vis spectra were recorded on a Cary Varian 50 spectrophotometer. The Vis-NIR spectra were recorded on a Perkin Elmer Lambda 1050 spectrophotometer. X-band EPR spectra were recorded on a Bruker EMX Plus spectrometer equipped with a Bruker nitrogen flow cryostat and a high sensitivity cavity. Electrochemical measurements were carried out using a Bio-Logic SP300 potentiostat. Experiments were performed in a standard three-electrode cell under argon atmosphere. A glassy carbon disc electrode (3 mm diameter), which was polished with 1 μm diamond paste, was used as the working electrode. For the electrolysis we used a carbon foam electrode. The auxiliary electrode is a platinum wire, while the reference was an $Ag/AgNO_3$ 0.01 M in CH_3CN. All the potentials are given vs. the Fc^+/Fc redox couple that was used as standard. The voltammetry curves were recorded at 298 K, whereas the electrolysis were conducted at 233 K.

Synthesis: H_4L_1. This ligand was synthesized according to a published procedure.[19]

2-Chloro-*N*-(3,5-di-*tert*-butyl-2-hydroxybenzyl)acetamide: To a stirred solution of 2,4-di-tert-butylphenol (1.03 g, 5 mmol) in acetic acid (10 mL) and sulfuric acid (2 mL), was added 2-chloro-N-(hydroxymethyl)acetamide (0.615 g, 5 mmol) dissolved in acetic acid (10 mL). After 8 h stirring, the reaction was stopped by addition of ice water (50 mL), resulting in the precipitation of a white solid. The precipitate was filtered off, washed with water, and dried under vaccum. Yield: 1.482 g (95%). ^{1}H NMR (400 MHz, DMSO) δ = 9.06 (s, 1H), 8.95 (s, 1H), 7.13 (d, J = 2.3 Hz, 1H), 7.03 (d, J = 2.4 Hz, 1H), 4.23 (d, J = 6.0 Hz, 2H), 4.18 (s, 2H), 1.34 (s, 9H), 1.23 (s, 9H). ^{13}C NMR (400 MHz, DMSO) δ = 168.44 (s), 151.67 (s), 141.32 (s), 136.98 (s), 125.53 (s), 125.11 (s), 123.08 (s), 42.73 (s), 35.14 (s), 34.32 (s), 31.91 (s), 30.17 (s). ESI-MS: m/z = 312.1 $[M+H]^+$.

2-(Aminomethyl)-4,6-di-tert-butylphenol: To a solution of 2-chloro-N-(3,5-di-tert-butyl-2-hydroxybenzyl)acetamide (0.775 g, 2.5 mmol) in ethanol (10 mL), was added hydrochloric acid (2 mL). The resulting solution was heated at reflux for 4 h. After cooling to room temperature, the solution was evaporated under vacuum. The pale-yellow solid was then dissolved in CH_2Cl_2 (50 mL). A saturated sodium bicarbonate solution was added into the solution. After 1 h stirring, the organic layer was collected, washed with water, and dried under vacuum. Yield: 0.531 g (90%). ^{1}H NMR (400 MHz, DMSO) δ = 7.05 (d, J = 2.3 Hz, 1H), 6.84 (d, J = 2.3 Hz, 1H), 3.91 (s, 2H), 1.35 (s, 9H), 1.22 (s, 9H). ^{13}C NMR (400 MHz, DMSO) δ = 154.74 (s), 140.11 (s), 124.27 (s), 123.62 (s), 122.12 (s), 44.14 (s), 34.95 (s), 34.25 (s), 31.98 (s), 30.07 (s). ESI-MS: m/z = 236.2 $[M+H]^+$.

H_4L_2: To a solution of 2-(aminomethyl)-4,6-di-tert-butylphenol (0.531 g 2.2 mmol) in methanol (5 mL), was added dropwise diethyl oxalate (0.165 g 1.1 mmol). After overnight stirring at RT, a white precipitate formed, which was collected by filtration and washed with cold methanol. Yield: 0.387 g (67%). ^{1}H NMR (400 MHz, DMSO) δ = 9.64 (s, 2H), 8.64 (s, 2H), 7.12 (d, J = 2.1 Hz, 2H), 7.05 (d, J = 2.1 Hz, 2H), 4.26 (d, J = 5.4 Hz, 4H), 1.34 (s, 18H), 1.20 (s, 18H). ^{13}C NMR (101 MHz, DMSO) δ = 160.39 (s), 150.92 (s), 141.04 (s), 136.75 (s), 124.96 (s), 124.72 (s), 122.60 (s), 34.65 (s), 33.78 (s), 31.37 (s), 29.71 (s). ESI-MS: m/z = 525.4 $[M+H]^+$.

$[Cu(L_1)](N(n\text{-}Bu)_4)_2$ ($1(N(n\text{-}Bu)_4)_2$): To a stirred solution of **H_4L_1** (50 mg, 0.1 mmol) in methanol (2 mL), was added tetrabutylammonium hydroxide (0.4 mL, 0.4 mmol). After 15 minutes, the solution of copper acetate monohydrate (20 mg, 0.1 mmol) in methanol (1 mL) was added to form a yellow solution. After 1 h stirring, the solution was filtered on celite, and evaporated under vacuum. A dark yellow solid was obtained. Yield: 92 mg (88%). Slow evaporation of a concentrate solution of the complex affords brown single crystals of **$1(N(n\text{-}Bu)_4)_2$**. ESI-MS: m/z = 555.1 $[M-2(n\text{-}Bu)_4N)]^-$.

$[Ni(L_1)](N(n\text{-}Bu)_4)$ ($2(N(n\text{-}Bu)_4)$): To a stirred solution of **H_4L_1** (50 mg, 0.1 mmol) in methanol (2 mL), was added tetrabutylammonium hydroxide (0.4 mL, 0.4 mmol). After stirring for 15 minutes, the solution of nickel acetate tetrahydrate (25 mg, 0.1 mmol) in methanol (1 mL) was added to form an orange solution. After 1 h stirring, the solution was filtered on celite, and evaporated under vacuum. A dark red solid was obtained. Yield: 98 mg (95%). Slow evaporation of a concentrate solution of the complex affords brown single crystals of **$2(N(n\text{-}Bu)_4)$**. ESI-MS: m/z = 550.1 $[M-(n\text{-}Bu)_4N]^-$.

$[Cu(L_2)]$ (3): To a stirred solution of **H_4L_2** (50 mg, 0.1 mmol) in methanol (2 mL), was added tetrabutylammonium hydroxide (0.4 mL, 0.4 mmol). The resulting solution was heated at reflux for 1 h, and the solution of copper acetate monohydrate (20 mg, 0.1 mmol) in methanol (1 mL) was added to form a dark red solution. After 1 h stirring, the solution was filtered on celite, and evaporated under vacuum. The raw product was purified over Sephadex LH-20 (15 g) with methanol as eluent. After evaporation of the solvent, the product was obtained as a dark red solid (16 mg, 27%). Slow evaporation of a concentrated solution of the complex affords dark red single crystals of **3**. APCI-MS: m/z = 582.3 $[M+H]^+$.

Crystal structure analysis. A single crystal was coated with a paraffin mixture, picked up with nylon loops and mounted in the nitrogen cold stream of a Nonius 4 circles diffractometer at 200 K. The Mo–Kα radiation (λ = 0.71073 Å) from an Incoatec micro Mo-target X-ray source equipped with Montel optics was used. The data were collected with a Bruker APEXII detector. Final cell parameters were obtained from refinements using the whole data. Intensities were corrected for Lorentz and polarisation effects using EVAL 14 and then for absorption using a multiscan method implemented with the program SADABS. The structures were solved and refined by charge flipping methods and subsequent difference Fourier techniques. SHELX implemented by the Olex2 software was used for the refinement.[33] All non-hydrogen atoms were anisotropically refined and hydrogen atoms were placed at calculated positions and refined as riding atoms with isotropic displacement parameters.

Deposition Numbers 2180498 (for **1**), 2180497 (for **2**), 2181720 (for **3**) contain the supplementary crystallographic data for this paper. These data are provided free of charge by the joint Cambridge Crystallographic Data Centre and Fachinformationszentrum Karlsruhe Access Structures service.

DFT Calculations: Full geometric optimizations were performed with the Gaussian 16.0 program.[34] The TPSSh[35] functional was used together with the Def2svp basis set[28] for the C,H,N,O atoms and the central metal ion. Solvent effects were included in all calculations via an implicit model of solvent (PCM) accounting for CH_2Cl_2.[28] Frequency calculations were systematically performed on the optimized structures in order to ensure that they correspond to a real energy minimum and not a saddle point. The ORCA software (release 3.0.1)[36] was used to calculate the EPR parameters (g-factors) on the above optimized structures. For this purpose the B3LYP functional was used, in combination with the RIJCOSX approximation.[37] An increased grid, as well as tight SCF and slow convergence criteria were used. The Def2-TZVP basis set[28a,38] was used for the atoms of the ligand, with a partially contracted core-property basis set CP(PPP)[39] for the nickel and copper ions. This basis set is based on the TurboMole DZ basis developed by Ahlrichs and coworkers and obtained from the basis set library under ftp.chemie.uni-karlsruhe.de/pub/basen. A complete mean field approach was used (Coulomb terms treated via RI). The isotropic and dipolar part of the HFC were calculated and relativistic effects were taken in account by using the ZORA Hamiltonian.[40] The zero field splitting parameters were calculated using the same functional/basis set, with the coupled-perturbated method and the

calculation of the SS term with a restricted spin-density from the singly occupied unrestricted natural orbitals. The Multiwfn was used to analyze orbital wavefunction and electron spin density.[41]

Catalysis: 0.6 mmol of an alcohol substrate and 0.72 mmol of potassium *tert*-butoxide (solid form) were introduced to a glass tube. 1 mL of a solution of the copper catalyst was added and the tube was immediately sealed with a septum and purged with oxygen using a syringe (3-time purge). The mixture was shaken at room temperature and aliquots of 30 µl were taken after 1, 3, 6 and 24 h. The tube is purged once with oxygen after the aliquots were collected before continuing the catalysis. The aliquots were directly dissolved in $CDCl_3$ for immediate ^{1}H NMR analysis (benzaldehyde detection) or extracted with water (detection of benzoate).

Acknowledgements

The authors thank the French National Research Agency in the framework of the "Investissements d'avenir" program (ANR-15-IDEX-02), Labex ARCANE and CBH-EUR-GS (ANR-17-EURE-0003) for financial supports. The authors are grateful to the Centre de Calcul Intensif en Chimie de Grenoble (CECIC) for providing the computational resources. The ICMG Platform (FR 2607) is acknowledged for the analytical support.

Conflict of Interest

The authors declare no conflict of interest.

Data Availability Statement

The data that support the findings of this study are available from the corresponding author upon reasonable request.

Keywords: Amidates · Copper · iminosemiquinone · Nickel · Phenoxyl ligands

[1] F. Thomas, in *Stable Radicals: Fundamentals and Applied Aspects of Odd-Electron Compounds* (Ed.: R. G. Hicks), John Wiley and Sons, Chichester, **2010**, pp. 281–316.

[2] a) C. T. Lyons, T. D. P. Stack, *Coord. Chem. Rev.* **2013**, *257*, 528–540; b) Y. Shimazaki, *Adv. Mater. Phys. Chem.* **2013**, *3*, 60–71; c) F. Thomas, *Dalton Trans.* **2016**, *45*, 10866–10877; d) R. M. Clarke, K. Herasymchuk, T. Storr, *Coord. Chem. Rev.* **2017**, *352*, 67–82; e) T. Storr, R. Mukherjee, *Inorg. Chem.* **2018**, *57*, 9577–9579; f) F. Thomas, *Eur. J. Inorg. Chem.* **2007**, *2007*, 2379–2404.

[3] a) N. Ito, S. E. V. Phillips, C. Stevens, Z. B. Ogel, M. J. McPherson, J. N. Keen, K. D. S. Yadav, P. F. Knowles, *Nature* **1991**, *350*, 87–90; b) P. F. Knowles, R. D. Brown, S. H. Koenig, S. Wang, R. A. Scott, M. A. McGuirl, D. E. Brown, D. M. Dooley, *Inorg. Chem.* **1995**, *34*, 3895–3902; c) J. W. Whittaker, *Chem. Rev.* **2003**, *103*, 2347–2364; d) J. W. Whittaker, *Arch. Biochem. Biophys.* **2005**, *433*, 227–239; e) D. Rokhsana, A. E. Howells, D. M. Dooley, R. K. Szilagyi, *Inorg. Chem.* **2012**, *51*, 3513–3524; f) D. Yin, S. Urresti, M. Lafond, E. M. Johnston, F. Derikvand, L. Ciano, J.-G. Berrin, B. Henrissat, P. H. Walton, G. J. Davies, H. Brumer, *Nat. Commun.* **2015**, *6*, 10197; g) R. E. Cowley, J. Cirera, M. F. Qayyum, D. Rokhsana, B. Hedman, K. O. Hodgson, D. M. Dooley, E. I. Solomon, *J. Am. Chem. Soc.* **2016**, *138*, 13219–13229; h) B. A. Jazdzewski, W. B. Tolman, *Coord. Chem. Rev.* **2000**, *200–202*, 633–685; i) P. Chaudhuri, K. Wieghardt, in *Prog. Inorg. Chem.*, **2001**, pp. 151–216; j) Y. Shimazaki, in *PATAI'S Chemistry of Functional Groups*, **2016**, pp. 1–26.

[4] H. Oshita, Y. Shimazaki, *Chem. Eur. J.* **2020**, *26*, 8324–8340.

[5] G. R. Dyrkacz, R. D. Libby, G. A. Hamilton, *J. Am. Chem. Soc.* **1976**, *98*, 626–628.

[6] a) T. Storr, E. C. Wasinger, R. C. Pratt, T. D. P. Stack, *Angew. Chem. Int. Ed.* **2007**, *46*, 5198–5201; *Angew. Chem.* **2007**, *119*, 5290–5293; b) T. Storr, P. Verma, R. C. Pratt, E. C. Wasinger, Y. Shimazaki, T. D. P. Stack, *J. Am. Chem. Soc.* **2008**, *130*, 15448–15459; c) M. Orio, O. Jarjayes, H. Kanso, C. Philouze, F. Neese, F. Thomas, *Angew. Chem. Int. Ed.* **2010**, *49*, 4989–4992; *Angew. Chem.* **2010**, *122*, 5109–5112; d) K. Asami, K. Tsukidate, S. Iwatsuki, F. Tani, S. Karasawa, L. Chiang, T. Storr, F. Thomas, Y. Shimazaki, *Inorg. Chem.* **2012**, *51*, 12450–12461; e) L. Chiang, A. Kochem, O. Jarjayes, T. J. Dunn, H. Vezin, M. Sakaguchi, T. Ogura, M. Orio, Y. Shimazaki, F. Thomas, T. Storr, *Chem. Eur. J.* **2012**, *18*, 14117–14127; f) A. Kochem, O. Jarjayes, B. Baptiste, C. Philouze, H. Vezin, K. Tsukidate, F. Tani, M. Orio, Y. Shimazaki, F. Thomas, *Chem. Eur. J.* **2012**, *18*, 1068–1072; g) A. Kochem, H. Kanso, B. Baptiste, H. Arora, C. Philouze, O. Jarjayes, H. Vezin, D. Luneau, M. Orio, F. Thomas, *Inorg. Chem.* **2012**, *51*, 10557–10571; h) K. Asami, A. Takashina, M. Kobayashi, S. Iwatsuki, T. Yajima, A. Kochem, M. van Gastel, F. Tani, T. Kohzuma, F. Thomas, Y. Shimazaki, *Dalton Trans.* **2014**, *43*, 2283–2293; i) L. Chiang, K. Herasymchuk, F. Thomas, T. Storr, *Inorg. Chem.* **2015**, *54*, 5970–5980; j) D. Martelino, S. Mahato, W. VandeVen, N. M. Hein, R. M. Clarke, G. A. MacNeil, F. Thomas, T. Storr, *J. Am. Chem. Soc.* **2022**, *144*, 11594–11607.

[7] a) Y. Shimazaki, T. D. P. Stack, T. Storr, *Inorg. Chem.* **2009**, *48*, 8383–8392; b) Y. Shimazaki, N. Arai, T. J. Dunn, T. Yajima, F. Tani, C. F. Ramogida, T. Storr, *Dalton Trans.* **2011**, *40*, 2469–2479; c) H. Kanso, R. M. Clarke, A. Kochem, H. Arora, C. Philouze, O. Jarjayes, T. Storr, F. Thomas, *Inorg. Chem.* **2020**, *59*, 5133–5148; d) R. Kunert, C. Philouze, F. Berthiol, O. Jarjayes, T. Storr, F. Thomas, *Dalton Trans.* **2020**, *49*, 12990–13002; e) H. Oshita, T. Yoshimura, S. Mori, F. Tani, Y. Shimazaki, O. Yamauchi, *J. Biol. Inorg. Chem.* **2018**, *23*, 51–59.

[8] a) F. C. Anson, T. J. Collins, T. G. Richmond, B. D. Santarsiero, J. E. Toth, B. G. R. T. Treco, *J. Am. Chem. Soc.* **1987**, *109*, 2974–2979; b) B. Cervera, J. L. Sanz, M. J. Ibanez, G. Vila, F. Lloret, M. Julve, R. Ruiz, X. Ottenwaelder, A. Aukauloo, S. Poussereau, Y. Journaux, M. Carmen Munoz, *J. Chem. Soc., Dalton Trans.* **1998**, 781–790; c) D. Dhar, G. M. Yee, T. F. Markle, J. M. Mayer, W. B. Tolman, *Chem. Sci.* **2017**, *8*, 1075–1085; d) L. L. Diaddario, W. R. Robinson, D. W. Margerum, *Inorg. Chem.* **1983**, *22*, 1021–1025; e) P. J. Donoghue, J. Tehranchi, C. J. Cramer, R. Sarangi, E. I. Solomon, W. B. Tolman, *J. Am. Chem. Soc.* **2011**, *133*, 17602–17605; f) P. Garrido-Barros, I. Funes-Ardoiz, S. Drouet, J. Benet-Buchholz, F. Maseras, A. Llobet, *J. Am. Chem. Soc.* **2015**, *137*, 6758–6761; g) M. R. Halvagar, W. B. Tolman, *Inorg. Chem.* **2013**, *52*, 8306–8308; h) J. Hanss, A. Beckmann, H. J. Kruger, *Eur. J. Inorg. Chem.* **1999**, 163–172; i) R. Ruiz, C. Surville-Barland, A. Aukauloo, E. Anxolabehere-Mallart, Y. Journaux, J. Cano, M. Carmen Munoz, *J. Chem. Soc., Dalton Trans.* **1997**, 745–752; j) T. Sakurai, J.-I. Hongo, A. Nakahara, Y. Nakao, *Inorg. Chim. Acta* **1980**, *46*, 205–210; k) A. Thibon-Pourret, F. Gennarini, R. David, J. A. Isaac, I. Lopez, G. Gellon, F. Molton, L. Wojcik, C. Philouze, D. Flot, Y. Le Mest, M. Réglier, N. Le Poul, H. Jamet, C. Belle, *Inorg. Chem.* **2018**, *57*, 12364–12375; l) K. J. Oliver, T. N. Waters, *J. Chem. Soc., Chem. Commun.* **1982**, 1111–1112.

[9] T. J. Collins, C. Slebodnick, E. S. Uffelman, *Inorg. Chem.* **1990**, *29*, 3433–3436.

[10] F. M. MacDonnell, N. L. P. Fackler, C. Stern, T. V. O'Halloran, *J. Am. Chem. Soc.* **1994**, *116*, 7431–7432.

[11] a) W. C. Ellis, N. D. McDaniel, S. Bernhard, T. J. Collins, *J. Am. Chem. Soc.* **2010**, *132*, 10990–10991; b) T. J. Collins, K. L. Kostka, E. Munck, E. S. Uffelman, *J. Am. Chem. Soc.* **1990**, *112*, 5637–5639; c) T. J. Collins, B. G. Fox, Z. G. Hu, K. L. Kostka, E. Munck, C. E. F. Rickard, L. J. Wright, *J. Am. Chem. Soc.* **1992**, *114*, 8724–8725.

[12] a) M. K. Coggins, M.-T. Zhang, A. K. Vannucci, C. J. Dares, T. J. Meyer, *J. Am. Chem. Soc.* **2014**, *136*, 5531–5534; b) F. T. de Oliveira, A. Chanda, D. Banerjee, X. Shan, S. Mondal, L. Que, E. L. Bominaar, E. Münck, T. J. Collins, *Science* **2007**, *315*, 835–838.

[13] a) F. C. Anson, T. J. Collins, R. J. Coots, S. L. Gipson, T. G. Richmond, *J. Am. Chem. Soc.* **1984**, *106*, 5037–5038; b) T. J. Collins, R. D. Powell, C. Slebodnick, E. S. Uffelman, *J. Am. Chem. Soc.* **1991**, *113*, 8419–8425.

[14] a) T. Corona, A. Draksharapu, S. K. Padamati, I. Gamba, V. Martin-Diaconescu, F. Acuña-Parés, W. R. Browne, A. Company, *J. Am. Chem. Soc.* **2016**, *138*, 12987–12996; b) T. Corona, F. F. Pfaff, F. Acuña-Parés, A. Draksharapu, C. J. Whiteoak, V. Martin-Diaconescu, J. Lloret-Fillol, W. R. Browne, K. Ray, A. Company, *Chem. Eur. J.* **2015**, *21*, 15029–15038;

c) T. J. Collins, T. R. Nichols, E. S. Uffelman, *J. Am. Chem. Soc.* **1991**, *113*, 4708–4709; d) A. G. Lappin, C. K. Murray, D. W. Margerum, *Inorg. Chem.* **1978**, *17*, 1630–1634.
[15] M. Eckshtain-Levi, R. Lavi, H. Arora, M. Orio, L. Benisvy, *Inorg. Chim. Acta* **2018**, *481*, 143–150.
[16] M. A. Hossain, F. Thomas, S. Hamman, E. Saint-Aman, D. Boturyn, P. Dumy, J.-L. Pierre, *J. Pept. Sci.* **2006**, *12*, 612–619.
[17] M. Eckshtain-Levi, R. Lavi, D. Yufit, M. Orio, R. Wanke, L. Benisvy, *Dalton Trans.* **2012**, *41*, 12457–12467.
[18] a) O. Rotthaus, O. Jarjayes, F. Thomas, C. Philouze, C. Perez Del Valle, E. Saint-Aman, J.-L. Pierre, *Chem. Eur. J.* **2006**, *12*, 2293–2302; b) L. Lecarme, L. Chiang, C. Philouze, O. Jarjayes, T. Storr, F. Thomas, *Eur. J. Inorg. Chem.* **2014**, *2014*, 3479–3487.
[19] U. Beckmann, E. Bill, T. Weyhermüller, K. Wieghardt, *Eur. J. Inorg. Chem.* **2003**, *2003*, 1768–1777.
[20] V. M. Jiménez-Pérez, C. Camacho-Camacho, Á. Ramos-Organillo, R. Ramírez-Trejo, A. Peña-Hueso, R. Contreras, A. Flores-Parra, *J. Organomet. Chem.* **2007**, *692*, 5549–5554.
[21] M. Güizado-Rodríguez, V. M. Jiménez-Pérez, J. E. Hernández-Rivera, J. M. Domínguez, R. Contreras, R. Quijada, *Polyhedron* **2007**, *26*, 4321–4327.
[22] E. Rufino-Felipe, J. Caballero-Jiménez, L.-G. Guerrero-Ramírez, M. Flores-Álamo, M.-Á. Muñoz-Hernández, *Inorg. Chem. Commun.* **2016**, *63*, 107–110.
[23] a) C. L. Simpson, S. R. Boone, C. G. Pierpont, *Inorg. Chem.* **1989**, *28*, 4379–4385; b) V. Bachler, *J. Comput. Chem.* **2009**, *30*, 2087–2098; c) J. Jacquet, E. Salanouve, M. Orio, H. Vezin, S. Blanchard, E. Derat, M. Desage-El Murr, L. Fensterbank, *Chem. Commun.* **2014**, *50*, 10394–10397; d) R. Rakshit, C. Mukherjee, *Eur. J. Inorg. Chem.* **2016**, 2731–2737; e) P. Chaudhuri, M. Hess, U. Flörke, K. Wieghardt, *Angew. Chem. Int. Ed.* **1998**, *37*, 2217–2220; *Angew. Chem.* **1998**, *110*, 2340–2343; f) P. Chaudhuri, M. Hess, J. Müller, K. Hildenbrand, E. Bill, T. Weyhermüller, K. Wieghardt, *J. Am. Chem. Soc.* **1999**, *121*, 9599–9610; g) P. Chaudhuri, K. Wieghardt, T. Weyhermüller, T. K. Paine, S. Mukherjee, C. Mukherjee, *Biol. Chem.* **2005**, *386*, 1023–1033.
[24] T. Takeyama, T. Suzuki, M. Kikuchi, M. Kobayashi, H. Oshita, K. Kawashima, S. Mori, H. Abe, N. Hoshino, S. Iwatsuki, Y. Shimazaki, *Eur. J. Inorg. Chem.* **2021**, *2021*, 4133–4145.
[25] Y. Shima, T. Suzuki, H. Abe, T. Yajima, S. Mori, Y. Shimazaki, *Chem. Commun.* **2022**, *58*, 6401–6404.
[26] a) A. Star, I. Goldberg, B. Fuchs, *J. Organomet. Chem.* **2001**, *630*, 67–77; b) V. Paredes-Garcia, D. Venegas-Yazigi, A. J. Lough, R. Latorre, *Acta Crystallogr. Sect. C* **2000**, *56*, e283.
[27] M. Rubčić, K. Užarević, I. Halasz, N. Bregović, M. Mališ, I. Đilović, Z. Kokan, R. S. Stein, R. E. Dinnebier, V. Tomišić, *Chem. Eur. J.* **2012**, *18*, 5620–5631.
[28] a) F. Weigend, R. Ahlrichs, *Phys. Chem. Chem. Phys.* **2005**, *7*, 3297; b) F. Weigend, *Phys. Chem. Chem. Phys.* **2006**, *8*, 1057–1065.
[29] a) E. R. Altwicker, *Chem. Rev. (Washington, DC, U.S.)* **1967**, *67*, 475–531; b) T. Yamaji, Saiful, M. Baba, S. Yamauchi, J. Yamauchi, *J. Phys. Chem. A* **2007**, *111*, 4612–4619; c) M. Orio, O. Jarjayes, B. Baptiste, C. Philouze, C. Duboc, J.-L. Mathias, L. Benisvy, F. Thomas, *Chem. Eur. J.* **2012**, *18*, 5416–5429.
[30] a) K. Wieghardt, W. Walz, B. Nuber, J. Weiss, A. Ozarowski, H. Stratemeier, D. Reinen, *Inorg. Chem.* **1986**, *25*, 1650–1654; b) B. De Castro, C. Freire, *Inorg. Chem.* **1990**, *29*, 5113–5119; c) F. Azevedo, M. A. A. F. D. C. T. Carrondo, B. de Castro, M. Convery, D. Domingues, C. Freire, M. T. Duarte, K. Nielsen, I. C. Santos, *Inorg. Chim. Acta* **1994**, *219*, 43–54; d) J. N. Stuart, A. L. Goerges, J. M. Zaleski, *Inorg. Chem.* **2000**, *39*, 5976–5984; e) V. B. Arion, P. Rapta, J. Telser, S. S. Shova, M. Breza, K. Lušpai, J. Kožišek, *Inorg. Chem.* **2011**, *50*, 2918–2931; f) A. Awasthi, I. F. Leach, S. Engbers, R. Kumar, R. Eerlapally, S. Gupta, J. E. M. N. Klein, A. Draksharapu, *Angew. Chem. Int. Ed.* **2022**, *61*, e202211345; g) Y. Shimazaki, F. Tani, K. Fukui, Y. Naruta, O. Yamauchi, *J. Am. Chem. Soc.* **2003**, *125*, 10512–10513; h) O. Rotthaus, O. Jarjayes, C. Perez Del Valle, C. Philouze, F. Thomas, *Chem. Commun.* **2007**, 4462–4464.
[31] M. M. Whittaker, J. W. Whittaker, *Biochemistry* **2001**, *40*, 7140–7148.
[32] M. M. Whittaker, P. J. Kersten, N. Nakamura, J. Sanders-Loehr, E. S. Schweizer, J. W. Whittaker, *J. Biol. Chem.* **1996**, *271*, 681–687.
[33] O. V. Dolomanov, L. J. Bourhis, R. J. Gildea, J. A. K. Howard, H. Puschmann, *J. Appl. Crystallogr.* **2009**, *42*, 339–340.
[34] M. J. Frisch, G. W. Trucks, H. B. Schlegel, G. E. Scuseria, M. A. Robb, J. R. Cheeseman, G. Scalmani, V. Barone, B. Mennucci, G. A. Petersson, H. Nakatsuji, M. Caricato, X. Li, H. P. Hratchian, A. F. Izmaylov, J. Bloino, G. Zheng, J. L. Sonnenberg, M. Hada, M. Ehara, K. Toyota, R. Fukuda, J. Hasegawa, M. Ishida, T. Nakajima, Y. Honda, O. Kitao, H. Nakai, T. Vreven, J. J. A. Montgomery, J. E. Peralta, F. Ogliaro, M. Bearpark, J. J. Heyd, E. Brothers, K. N. Kudin, V. N. Staroverov, R. Kobayashi, J. Normand, K. Raghavachari, A. Rendell, J. C. Burant, S. S. Iyengar, J. Tomasi, M. Cossi, N. Rega, J. M. Millam, M. Klene, J. E. Knox, J. B. Cross, V. Bakken, C. Adamo, J. Jaramillo, R. Gomperts, R. E. Stratmann, O. Yazyev, A. J. Austin, R. Cammi, C. Pomelli, J. W. Ochterski, R. L. Martin, K. Morokuma, V. G. Zakrzewski, G. A. Voth, P. Salvador, J. J. Dannenberg, S. Dapprich, A. D. Daniels, Ö. Farkas, J. B. Foresman, J. V.Ortiz, J. Cioslowski, D. J. Fox, *Gaussian 09*, *Revision D.01*, Gaussian, Inc., Wallingford CT, **2009**.
[35] a) J. M. Tao, J. P. Perdew, V. N. Staroverov, G. E. Scuseria, *Phys. Rev. Lett.* **2003**, *91*, 146401; b) V. N. Staroverov, G. E. Scuseria, J. Tao, J. P. Perdew, *J. Chem. Phys.* **2003**, *119*, 12129–12137.
[36] F. Neese, *WIREs Comput. Mol. Sci.* **2012**, *2*, 73–78.
[37] F. Neese, G. Olbrich, *Chem. Phys. Lett.* **2002**, *362*, 170–178.
[38] D. A. Pantazis, X.-Y. Chen, C. R. Landis, F. Neese, *J. Chem. Theory Comput.* **2008**, *4*, 908–919.
[39] X. Sun, H. Chun, K. Hildenbrand, E. Bothe, T. Weyhermüller, F. Neese, K. Wieghardt, *Inorg. Chem.* **2002**, *41*, 4295–4303.
[40] C. van Wüllen, *Int. J. Quantum Chem.* **1996**, *58*, 147–152.
[41] T. Lu, F. Chen, *J. Comput. Chem.* **2012**, *33*, 580–592.

Manuscript received: December 21, 2022
Revised manuscript received: February 27, 2023
Accepted manuscript online: March 6, 2023